HHS Public Access

Author manuscript

Nature. Author manuscript; available in PMC 2017 March 01.

Published in final edited form as:

Nature. 2016 September 01; 537(7618): 117–121. doi:10.1038/nature19102.

Structural basis for inhibition of a voltage-gated Ca^{2+} channel by Ca^{2+} antagonist drugs

Lin Tang[1,2], **Tamer M. Gamal El-Din**[1], **Teresa M. Swanson**[1], **David C. Pryde**[3], **Todd Scheuer**[1], **Ning Zheng**[1,2,§], and **William A. Catterall**[1,§]

[1]Department of Pharmacology, University of Washington, Seattle, Washington 98195-7280, USA

[2]Howard Hughes Medical Institute, University of Washington, Seattle, Washington 98195-7280, USA

[3]Curadev Pharma, Discovery Park, Sandwich, Kent CT14 9FF, UK

Abstract

Ca^{2+} antagonist drugs are widely used in therapy of cardiovascular disorders[1,2]. Three chemical classes of drugs bind to three separate, but allosterically interacting, receptor sites on $Ca_V1.2$ channels, the most prominent voltage-gated Ca^{2+} (Ca_V) channel type in myocytes in cardiac and vascular smooth muscle[3–9]. The 1,4-dihydropyridines are used primarily for treatment of hypertension and angina pectoris and are thought to act as allosteric modulators of voltage-dependent Ca^{2+} channel activation, whereas phenylalkylamines and benzothiazepines are used primarily for treatment of cardiac arrhythmias and are thought to physically block the pore[1,2]. The structural basis for the different binding, action, and therapeutic uses of these drugs remains unknown. Here we present crystallographic and functional analyses of drug binding to the bacterial homotetrameric model Ca_V channel Ca_VAb, which is inhibited by dihydropyridines and phenylalkylamines with nanomolar affinity in a state-dependent manner. The binding site for amlodipine and other dihydropyridines is located on the external, lipid-facing surface of the pore module, positioned at the interface of two subunits. Dihydropyridine binding allosterically induces an asymmetric conformation of the selectivity filter, in which partially dehydrated Ca^{2+} interacts

---

Correspondence and requests for materials should be addressed to N.Z. (nzheng@uw.edu) or W.A.C. (wcatt@uw.edu).
§These authors jointly supervised this work.

Author Information The coordinates and structure factors have been deposited in the Protein Data Bank with the following accession codes 5KLB (CavAb, 5 mM Ca^{2+} 2.7Å; 5KLG (CavAb-W195Y-UK-59811, 5 mM Ca^{2+}); 5KLS (CavAb-UK-59811, 5 mM Ca^{2+}); 5KMD (CavAb-W195Y-amlodipine, 5 mM Ca^{2+}); 5KMF (CavAb-W195Y nimodipine, 5 mM Ca^{2+}); and 5KMH (CavAb-Br-verapamil, 5 mM Ca^{2+}).

Author Contributions L.T., T.M.G., T.M.S., T.S., D.C.P., N.Z., and W.A.C. designed the experiments. D.C.P. provided compound UK-59811. L.T. conducted protein purification, crystallization, and X-ray diffraction experiments for dihydropyridines. L.T. and T.M.S. conducted protein purification, crystallization, and X-ray diffraction experiments for Br-verapamil. L.T. and T.M.S. determined the structures and analysed the structural results with input from T.M.G. and N.Z. T.M.G. designed and analysed mutants that block drug binding and performed all of the electrophysiological studies. T.M.G., T.S., and W.A.C. analysed the electrophysiological results. All authors contributed to the interpretation of the structures in light of the physiological data. L.T., N.Z., and W.A.C. wrote the manuscript with input from all co-authors.

The authors declare no competing financial interests. Readers are welcome to comment on the online version of the paper.

Online Content Methods, along with any additional Extended Data display items and Source Data, are available in the online version of the paper; references unique to these sections appear only in the online paper.

Supplementary Information is available in the online version of the paper.

directly with one subunit and blocks the pore. In contrast, the phenylalkylamine Br-verapamil binds in the central cavity of the pore on the intracellular side of the selectivity filter, physically blocking the ion-conducting pathway. Structure-based mutations of key amino-acid residues confirm drug binding at both sites. Our results define the structural basis for binding of dihydropyridines and phenylalkylamines at their distinct receptor sites on Ca_V channels and offer key insights into their fundamental mechanisms of action and differential therapeutic uses in cardiovascular diseases.

Ca_V1 channels are composed of a complex of a pore-forming α1 subunit associated with β, γ, and α2δ subunits[1,10]. The α1 subunits contain four homologous domains with six transmembrane segments in each[11,12]. Transmembrane segments S1–S4 form the voltage-sensing module, and S5, S6 and the intervening P-loop form the pore[1]. The overall architecture of the mammalian skeletal muscle $Ca_V1.1$ channel was recently elucidated at a resolution of ~4–6 Å by cryo- electron microscopy[13]. However, higher-resolution structural analysis of mammalian Ca_V channels has not yet been achieved. The bacterial voltage-gated Na^+ channel NaChBac and its relatives are homote-trameric proteins composed of four identical subunits, each analogous to one domain of a mammalian voltage-gated Na^+ or Ca^{2+} channel[14,15]. These bacterial channels probably represent the evolutionary ancestors of both mammalian channel families. The structures of bacterial Na^+ channels have been determined at high resolution by X-ray crystallography in pre-open[16] and inactivated[17,18] states. Moreover, the structural basis for Ca^{2+} conductance and selectivity has been elucidated at atomic resolution through studies of Ca_VAb, a site-directed mutant of Na_VAb with full Ca^{2+} channel function[19]. We have used derivatives of Ca_VAb (see Methods) to define receptor sites and mechanisms of action of Ca^{2+} antagonist drugs at atomic resolution.

Ca_VAb was inhibited by amlodipine with high affinity (Fig. 1a–c). No inhibition was observed during single depolarizations, indicating that amlodipine does not enter the open pore and block it (Fig. 1a). However, inhibition increased progressively during trains of depolarizations, reflecting increased binding affinity for the activated and/or inactivated states of Ca_VAb (Fig. 1b). After a train of 20 depolarizing pulses, the half-maximum inhibitory concentration (IC_{50}) for inhibition by amlodipine was 10 nM (Fig. 1c). This affinity was surprisingly high, considering the evolutionary distance between Ca_VAb and mammalian $Ca_V1.2$ channels, which have IC_{50} values from 0.3 nM to 1 μM for various dihydropyridines[20].

Photoaffinity labelling and site-directed mutagenesis suggest that dihydropyridines bind to a receptor site at the interface of homologous domains III and IV and the adjacent pore module in domain III in $Ca_V1.2$ channels4–7,21,22. In Ca_VAb, four identical subunits form a homotetramer (Fig. 1d)[19]. The structure of the amlodipine–Ca_VAb complex reveals the antagonist bound on the outer, lipid-facing surface of the pore module in the intersubunit crevice formed by neighbouring tilted S6 helices and the P-helix of the selectivity filter (Fig. 1d, e, yellow sticks). Despite the homotetrameric structure of Ca_VAb, only a single drug-binding site per tetramer is occupied, suggesting that drug-induced conformational changes prevent occupancy of more than one site. Amino-acid residues Y195, I199, F171, Y168 and F167 form a hydrophobic pocket for interaction with amlodipine (Fig. 1f). The

dihydropyridine ring is sandwiched between Y195 of S6 and F167 of the P-loop. F171 and I199 of S6 form the bottom of the cleft that accommodates the bound drug. Mutations of I199 (for example, I199S) had minimal effects on Ca_VAb function (Extended Data Fig. 1), but markedly reduced the affinity for amlodipine (IC_{50} = 112 nM; Fig. 1c).

Nimodipine inhibited Ca_VAb like amlodipine, but its IC_{50} was 100 nM (Fig. 2a–c). Nimodipine binds to the same site as amlodipine (Fig. 2d, e and Extended Data Fig. 2a, b). The substitution I199S increased the IC_{50} for nimodipine from 100 nM to 5.7 μM (Fig. 2c), and W195Y increased it to 508 nM (Extended Data Fig. 3). The experimental Br-dihydropyridine derivative UK-59811 inhibited Ca_VAb with IC_{50} = 194 nM (Extended Data Fig. 4) and bound in a similar position (Fig. 2f and Extended Data Fig. 2a, c). Anomalous scattering density from its Br atom further confirmed the location of the dihydropyridine-binding site at the interface between the S6 segments of two adjacent subunits surrounded by Y195, F171, F167, and I199 (Fig. 2f, green mesh). High-resolution structures of Ca_VAb revealed 16 molecules of bound lipid per tetramer[19]. Without drugs, we found a single molecule of DMPC lipid aligned in the dihydropyridine-binding pocket with its polar headgroup facing the extracellular side and its long hydrocarbon tails projecting deep into the crevice formed by neighbouring S6 helices (Fig. 2g and Extended Data Fig. 2d). Thus, our structures reveal that dihydropyridine binding displaces an endogenous lipid molecule from their common binding site on Ca_VAb.

In the absence of dihydropyridines, the Ca_VAb structure has fourfold symmetry around the pore axis[19]. Four lipid molecules are found in the central cavity, occupying fenestrations that connect to the exterior of the channel (Fig. 3a). Binding of dihydropyridines to Ca_VAb rearranges the quaternary structure and breaks the fourfold symmetry (Fig. 3c, e, g, compare shaded cross-sections; see Supplementary Discussion of asymmetry induced by drug binding). With drug bound, the four lipid molecules in the central cavity lose their symmetric spatial organization, and the fenestration closest to the drug-binding site is no longer occupied by a lipid chain.

By introducing asymmetry, dihydropyridine binding triggers allosteric changes at the selectivity filter of Ca_VAb and alters binding of the substrate ion. There are three Ca^{2+}-binding sites in the Ca_VAb selectivity filter: two high-affinity sites (Sites 1 and 2) followed by one lower-affinity site (Site 3) arranged sequentially from its extracellular to intracellular end[19]. Without drug, Ca^{2+} binds near the central axis of the pore in a fully hydrated state, coordinated symmetrically by four D178 carboxylate side chains (Fig. 3b)[19]. With dihydropyridines bound, Ca^{2+} binds to Site 1 asymmetrically in a partially dehydrated state —significantly off the central axis of the pore and closer to one or two D178 carboxylate groups at a distance of 2.8–3.3 Å (Fig. 3d, f, h and Extended Data Fig. 5a–d). This binding distance suggests direct interaction of bound Ca^{2+} with the carboxylate side chain (Supplementary Discussion). In contrast, binding of Ca^{2+} at Site 2 is unchanged (data not shown). The anomalous scattering density of Ca^{2+} confirms its off-axis location in Site 1 and on-axis location in Site 2 (Extended Data Fig. 5e, f).

Studies with quaternary phenylalkylamine analogues revealed that these drugs inhibit $Ca_V1.2$ channels only after cytoplasmic application, and that drug binding is increased by

repetitive depolarization to open the pore[2,23]. It was therefore concluded that tertiary phenylalkylamines such as verapamil penetrate the membrane in uncharged form, are re-protonated in the cytosol, and block the $Ca_V1.2$ channel by entering the intracellular mouth of the open pore in their protonated form and binding to their receptor site[2,23]. Photoaffinity labelling and site-directed mutagenesis revealed that the phenylalkylamine receptor site is formed by S6 segments in domains III and IV of $Ca_V1.2$ channels, consistent with drug binding in the pore[4–7,24,25].

When Br-verapamil was perfused at −120 mV, the first depolarization to 0 mV showed progressive reduction of the current during the pulse (Fig. 4a). This profile supports a pore-blocking mechanism, in which the drug progressively enters and blocks the open pore. Repetitive depolarizing stimuli increased inhibition of Ca_VAb by Br-verapamil (Fig. 4b), yielding IC_{50} values of 810 nM for Br-verapamil (Fig. 4c, blue squares) and 475 nM for verapamil (Extended Data Fig. 6a, b) at steady state. The action of these drugs is strikingly state- dependent: the IC_{50} for Br-verapamil in the resting state is 24 μM, 30-fold higher than observed after a train of depolarizing stimuli (Fig. 4c, blue circles).

Our crystal structures revealed a single molecule of Br-verapamil bound in the central cavity on the intracellular side of the ion selectivity filter (Fig. 4d, e; see Supplementary Discussion of asymmetry induced by drug binding). The bound drug is oriented with its characteristic positively charged tertiary amino group facing in the extracellular direction pointing towards Site 3 in the selectivity filter. In this position, the bound phenylalkylamine would physically block the pore. The distance between the tertiary amino group and Ca^{2+} coordinated by the carbonyls of L176 is 5 Å. The methoxy groups in the aromatic rings are located close to the inner end of the fenestrations, surrounded by T206, M209 of the neighbouring subunit and T175, M174, L176 of the selectivity filter (Fig. 4f). The two aromatic rings of Br-verapamil interact with T206 residues from two neighbouring S6 helices (Fig. 4f). A view from the intracellular side shows that Br-verapamil binds closer to two subunits on one side of the pore (Fig. 4f). The anomalous scattering from Br-verapamil further defines the position of the aromatic ring that is farther from the amino group and confirms its interaction with T206 (Fig. 4e, green mesh). Mutations in T206 impair inactivation of Ca_VAb (Extended Data Fig. 6c, e) and markedly reduce the affinity for Br-verapamil. For example, the conservative mutation T206S increases the IC_{50} for state-dependent inhibition from 810 nM to 24 μM (Fig. 4c, red squares) and the IC_{50} for resting state inhibition of Ca_VAb from 24 μM to 115 μM (Fig. 4c, red circles). The effects of these mutations on both resting and state-dependent block confirm that there is a direct interaction between the drug and T206. These results define the receptor site for pore block by phenylalkylamines at high resolution. Similar to the dihydropyridine-binding site, the phenylalkylamine-binding site is also occupied by lipid molecules in the absence of the drug.

At concentrations above 1 μM, dihydropyridines inhibit voltage-gated Na^+ channels in a manner consistent with pore block[26]. At the high drug concentrations used in our crystallization studies, we found binding of UK-59811 (Fig. 4g–i) and other dihydropyridines in the pore of Ca_VAb. The anomalous scattering density of its Br places the dihydropyridine ring deep in the central cavity where it forms hydrophobic contacts with two neighbouring subunits (Fig. 4h, green mesh). Compared to Br-verapamil, UK-59811

bound more towards the intracellular base of the central cavity and was located closer to one subunit (Fig. 4g–i). Low-affinity block of Na^+ channels by dihydropyridines bound in this site may contribute to cardiac arrhythmias caused by toxic overdoses of these drugs.

Overall, our results provide a structural basis for understanding how dihydropyridines and phenylalkylamines bind at two distinct, but allosterically coupled receptor sites on $Ca_V1.2$ channels and have different efficacy for treatment of hypertension and angina pectoris versus cardiac arrhythmias[1–3,5–7]. Consistent with photoaffinity-labelling and site-directed mutagenesis[5–7], dihydropyridines bind on the outer, lipid-facing surface of the pore module at the interface between two subunits of Ca_VAb, in analogy with their proposed site of action between domains III and IV of $Ca_V1.2$ channels4,21. Their binding site is exposed to the extracellular side of the membrane, but not to the intracellular side. These structural results reveal why charged dihydropyridines are ineffective when applied intracellularly[27], and they are consistent with location of the drug-binding site ~11–14 Å from the outer surface of the lipid bilayer as inferred from studies of charged derivatives of amlodipine with hydrophobic linkers of increasing length[28]. These comparisons reveal a close analogy between the site of dihydropyridine binding in our crystal structures of Ca_VAb and the expectations from studies of $Ca_V1.2$ channels, but the exact position of the drug-binding site in Ca_VAb is approximately one helical turn towards the extracellular side from the amino-acid residues implicated in dihydropyridine binding by studies of $Ca_V1.2$ channels (Extended Data Fig. 7). This difference may reflect the great evolutionary distance between Ca_VAb and mammalian Ca_V channels and/or indirect allosteric effects of mutations studied in Ca_V1 channels.

Binding of a single dihydropyridine to Ca_VAb induces a conformational change that alters the fourfold symmetry of the quaternary structure and induces changes in the three unoccupied dihydropyridine-binding sites that may prevent drug occupancy (Extended Data Fig. 8). Drug binding also disrupts the symmetry of the ion selectivity filter, allowing direct coordination of Ca^{2+} by carboxylate side chains. This conformational change is mediated in part by an altered pattern of hydrogen bonds formed by N181 in the subunit binding the dihydropyridine (Fig. 3). These structural results correlate closely with ligand-binding studies of $Ca_V1.2$ channels, which suggested that dihydropyridines induce high-affinity Ca^{2+} binding and block of the pore[29,30]. Our structural studies reveal exactly how dihydropyridines act as indirect allosteric blockers of the pore of Ca^{2+} channels. Dihydropyridine binding to $Ca_V1.2$ channels is voltage-dependent because of the high affinity for the inactivated state[1,5–7]. In a remarkable parallel, dihydropyridine binding causes a conformational change to an asymmetric pore structure in Ca_VAb, which is similar to the asymmetry induced in inactivated states of the parent Na_VAb channel17 and its relative Na_VRh18. Dihydropyridine binding may induce a similar asymmetric, Ca^{2+}-blocked state of $Ca_V1.2$ channels and thereby enhance their inactivation, allowing selective inhibition in persistently depolarized cells. This mechanism underlies the use of dihydropyridines in treatment of hypertension and angina pectoris, in which vascular smooth muscle cells of resistance vessels are persistently depolarized, and their $Ca_V1.2$ channels are selectively inhibited by dihydropyridines.

The phenylalkylamine receptor site was localized to the S6 segments in domains III and IV of $Ca_V1.2$ channels by photoaffinity labelling and mutational analysis, and it was proposed

that the amino-acid side chains involved in drug binding point towards the lumen of the pore[4–6,24,25]. Our structural results correlate precisely with this expectation and reveal the exact structure of the drug–receptor complex. Br-verapamil is stretched between two subunits of Ca_VAb, consistent with drug binding at the interface of domains III and IV in Ca_V1.2 channels[4–6,24,25]. As for dihydropyridines, phenylalkylamine binding at this site disrupts the fourfold symmetry of the pore (Extended Data Fig. 9). Location of the phenylalkylamine receptor site deep in the central cavity in the pore reveals why binding of these drugs is state-dependent. Access of phenylalkylamines to their receptor is greatly enhanced by opening the intracellular activation gate, which allows diffusion to the drug receptor site. Drug binding is therefore frequency-dependent, allowing selective block of Ca_V1.2 channels in rapidly firing cardiac myocytes[2]. This mechanism is the basis for use of verapamil for cardiac arrhythmias.

Overall, our structural studies illuminate the complex pharmacology and therapeutic uses of Ca^{2+} antagonist drugs in treatment of different cardiovascular disorders at the atomic level (see Supplementary Discussion). These structural models will be important for design and development of next-generation Ca^{2+} antagonist drugs to provide safer and more effective treatment of hypertension, angina pectoris, cardiac arrhythmia, and other medical conditions.

METHODS

Ca_VAb constructs and drugs

As originally defined, Ca_VAb was constructed by introducing the mutations E177D, S178D and M181D as a triple mutant into Na_VAb19. This construct was used for all electrophysiological studies, except as noted in figure legends. In this work, we have also used Ca_VAb E177D S178D M181N, which has an identical structure and Ca^{2+}-binding properties and has high Ca^{2+} selectivity[19]. It gives greater consistency of high-resolution crystal structures. We have also added the mutation W195Y, which substitutes the Y residue from the analogous position in mammalian Ca_V1.1 channels for W195 in Ca_VAb. This mutant gives better resolution of drugs bound at the dihydropyridine site. Ca_VAb E177D S178D M181N W195Y was used for all structural studies presented here, except as noted in the figure legends. Similar structural results were obtained for both versions of Ca_VAb. We found that amlodipine and other dihydropyridines (Figs. 1 and 2 and Extended Data Figs 1, 3 and 4) and verapamil and other phenylalkylamines (Fig. 4 and Extended Data Fig. 6) effectively blocked Ca_VAb and gave high-resolution crystal structures; however, we were unable to prepare crystals with bound diltiazem for structural biology so we have not addressed the structure of the benzothiazepine receptor site in this work.

Electrophysiology

All measurements were done in insect cells (*Trichoplusia ni* cells; High5). All Ca_VAb constructs used were made on the background of N49K mutation. Mutation N49K shifts the activation curve ~75 mV to more positive potentials compared to wild-type Ca_VAb and abolishes the use-dependent inactivation as described previously[19,31]. All constructs showed good expression, allowing measurement of ionic currents 24–48 h after infection. Whole-

cell Ba^{2+} currents were recorded using an Axopatch 200 amplifier (Molecular Devices) with glass micropipettes (2–4 MΩ). Capacitance was subtracted and 80–90% of series resistance was compensated using internal amplifier circuitry. Extracellular solution contained in (mM) 10 $BaCl_2$, 140 NMDG-methanesulphonate, 20 HEPES, (pH 7.4, adjusted with $Ba(OH)_2$, $[Ba^{2+}]_{total}$ = 13 mM). Intracellular solution contained in (mM) 105 CsF, 35 NaCl, 10 HEPES, 10 EGTA, (pH 7.4, adjusted with CsOH). Current–voltage (*I–V*) relationships were recorded in response to steps to voltages ranging from −120 to +50 mV in 10-mV increments from a holding potential of −120 mV. Conductance-voltage (*G–V*) curves were calculated from the corresponding (*I–V*) curves. Pulses were generated and currents were recorded using Pulse software controlling an Instrutech ITC18 interface (HEKA). Data were analysed using Igor Pro 6.2 (WaveMetrics). Sample sizes were chosen to give s.e.m. values of less than 10% of peak values based on prior experimental experience. Inhibition curves were fit with a Hill equation with n_H = 1.0 unless indicated otherwise in the figure legends.

Protein expression and purification

The pFastBac-Flag-Ca_VAb was used as the construct for producing homotetrameric model voltage-gated Ca^{2+} channel[19]. I199S, W195Y, and T206S constructs were generated via site-directed mutagenesis using QuickChange (Stratagene). Recombinant baculovirus were produced using the Bac-to-Bac system (Invitrogen), and *T. ni* insect cells were infected for large-scale protein purification. Cells were harvested 72 h post-infection and re-suspended in buffer A (50 mM Tris-HCl, pH = 8.0, 200 mM NaCl) supplemented with protease inhibitors and DNase. After sonication, digitonin (EMD Biosciences) was added to 1%, and solubilization was carried out for 1–2 h at 4 °C. Clarified supernatant was then incubated with anti-Flag M2-agarose resin (Sigma) for 1–2 h at 4 °C with gentle mixing. Flag-resin was washed with ten column volumes of buffer B (buffer A supplemented with 0.12% digitonin) and eluted with buffer B supplemented with 0.1 mg ml^{-1} Flag peptide. The eluant was concentrated and then passed over a Superdex 200 column (GE Healthcare) in 10 mM Tris-HCl pH =8.0, 100 mM NaCl and 0.12% digitonin. The peak fractions were concentrated using a Vivaspin 30K centrifugal device.

Crystallization and data collection

Ca_VAb and the W195Y mutant were concentrated to ~20 mg ml^{-1} and reconstituted into DMPC:CHAPSO (Anatrace) bicelles according to standard protocols[16,17,32,33]. The protein-bicelle preparation and a well solution containing 1.8–2.0 M ammonium sulphate, 100 mM Na-citrate pH = 5.0 was mixed in 1:1 ratio and set up in a hanging-drop vapour-diffusion format. All the antagonist complex crystals were obtained through co-crystallization by incubating the protein-bicelle with 100 μM antagonist overnight before setting up crystallization trials. For the UK-59811 complex, both 100 μM and 200 μM antagonist were used for UK-59811/Ca_VAb crystals. Crystals were cryoprotected by soaking in 0.1 M Na-acetate, pH 5.0, 26% glucose, 2.0 M ammonium sulphate, and 5 mM Ca^{2+}. Crystals were plunged into liquid nitrogen and maintained at 100 K during all data collection procedures.

The anomalous diffraction data sets for Br were collected at 0.9194 Å, and the anomalous data sets for Ca^{2+} were collected at 1.75 Å with the same synchrotron radiation source

(Advanced Light Source, BL8.2.1). To optimize the anomalous scattering signal, the data sets were collected by using the 'inverse beam strategy' with the wedge size of 5°.

Structure determination, refinement, and analysis

X-ray diffraction data were integrated and scaled with the HKL2000 package[34] and further processed with the CCP4 package[35]. The structure of Ca_VAb and its antagonist complex were solved by molecular replacement using an individual subunit of the Ca_VAb structure (PDB code 4MS2) as the search template. The data sets were processed in P21221 space group, in which there are four molecules in one asymmetric unit. Crystallography and NMR System software[36] were used for refinement of coordinates and *B*-factors. Final models were obtained after several cycles of refinement with REFMAC[37] and PHENIX[38] plus manual re-building using COOT[39]. The geometries of the final structural models of Ca_VAb and its antagonist complexes were verified using PROCHECK[40]. Divalent cations were identified by anomalous difference Fourier maps calculated using data collected at wavelengths of 1.75 Å for Ca^{2+}. The Br atoms of UK-59811 and Br-verapamil were identified by anomalous difference Fourier maps calculated using data collected at wavelengths of 0.9194 Å. Procedures accounting for merohedral twinning were performed during structural refinement of amlodipine, nimodipine, and Br-verapamil data sets. Detailed crystallographic data and refinement statistics for all constructs are shown in Extended Data Table 1. All structural figures were prepared with PyMol[41].

Extended Data

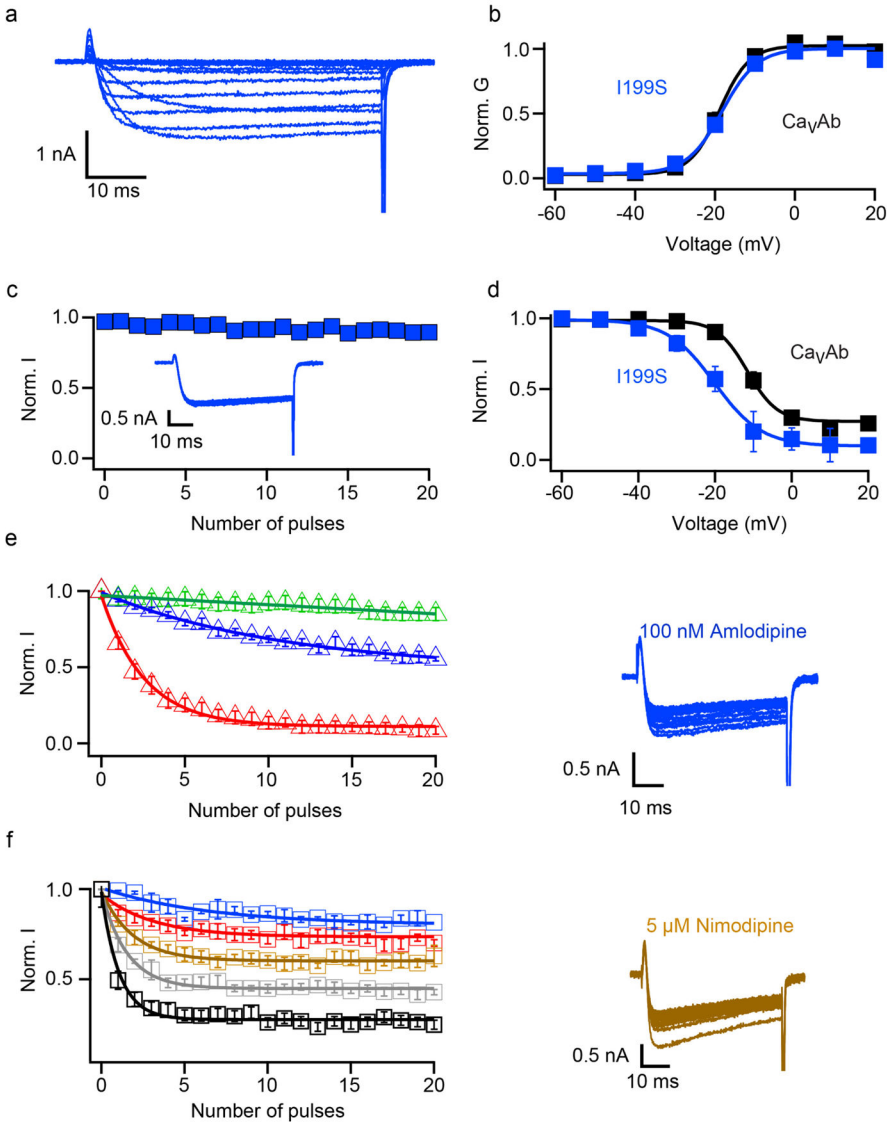

Extended Data Figure 1. Biophysical characterization of Ca_VAb I199S

a, Ba^{2+} currents recorded from a holding potential of −120 mV to test potentials from −60 mV to 20 mV in 10 mV steps for I199S. **b**, *G*–*V* curves of Ca_VAb and Ca_VAb I199S derived from peak *I*–*V* relationships. The voltages for half-maximal activation and slopes are: Ca_VAb: $V_{1/2}$ = − 18.8±0.3, k =3.68±0.43, n = 7; Ca_VAb I199S: $V_{1/2}$ = −18.8±0.3, k =3.88±0.47 (n = 5). **c**, Repetitive depolarization to 0 mV at 1 Hz from a holding potential of − 120mV (n 5). **d**, Steady-state inactivation of Ca_VAb and Ca_VAb I199S. Two pulses were applied: a 300-ms conditioning pulse to the indicated potentials followed by 50-ms test pulse to 0 mV (n =3). **e**, State-dependent block of Ca_VAb I199S by 10 nM (green), 100 nM (blue), or 1.5 μM (red) amlodipine during repetitive depolarizations to 0 mV (left, n = 3–5 cells). Ba^{2+} currents in 100 nM amlodipine for Ca_VAb I199S (right). **f**, Concentration-dependent block of Ca_VAb I199S by nimodipine at 100 nM (blue), 1 μM (red), 5 μM (brown), 10 μM

(grey) and 50 μM (black) (left, n = 4–5 cells for each curve). Ba^{2+} currents in the presence of 5 μM nimodipine for Ca_VAb I199S (right).

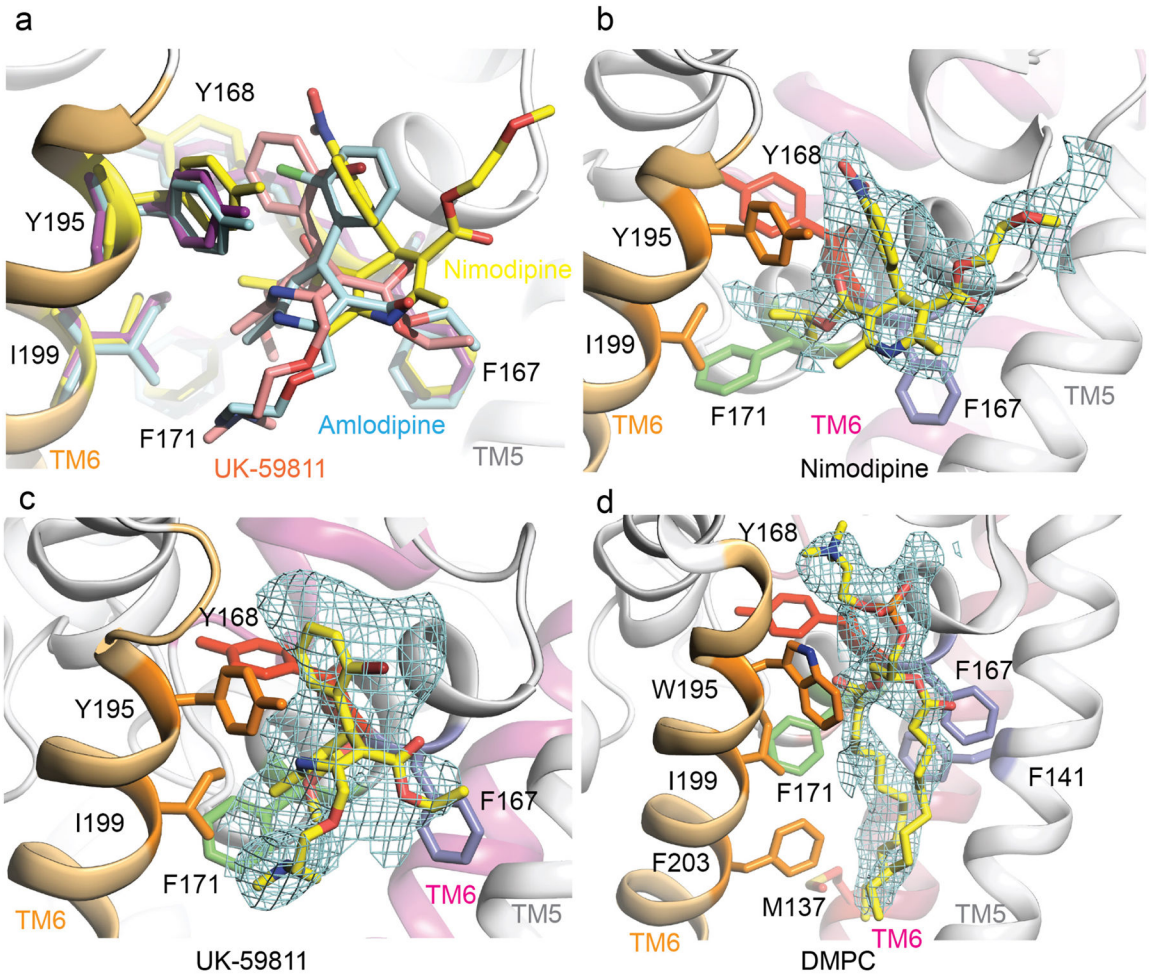

Extended Data Figure 2. Structural comparison of the binding modes of amlodipine, nimodipine, and UK-59811

a, Superposition of Ca_VAb in complexes with amlodipine (cyan), nimodipine (yellow), and UK-59811 (magenta) at the dihydropyridine binding site viewed from the side of the pore module. The side chains of dihydropyridine-interacting residues are shown in sticks. **b**, An *F*o–*F*c simulated annealing omit map contoured at 2.5σ for nimodipine. **c**, An *F*o–*F*c simulated annealing omit map contoured at 2.5σ for UK-59811. **d**, An *F*o–*F*c simulated annealing omit map contoured at 2.5σ for DMPC.

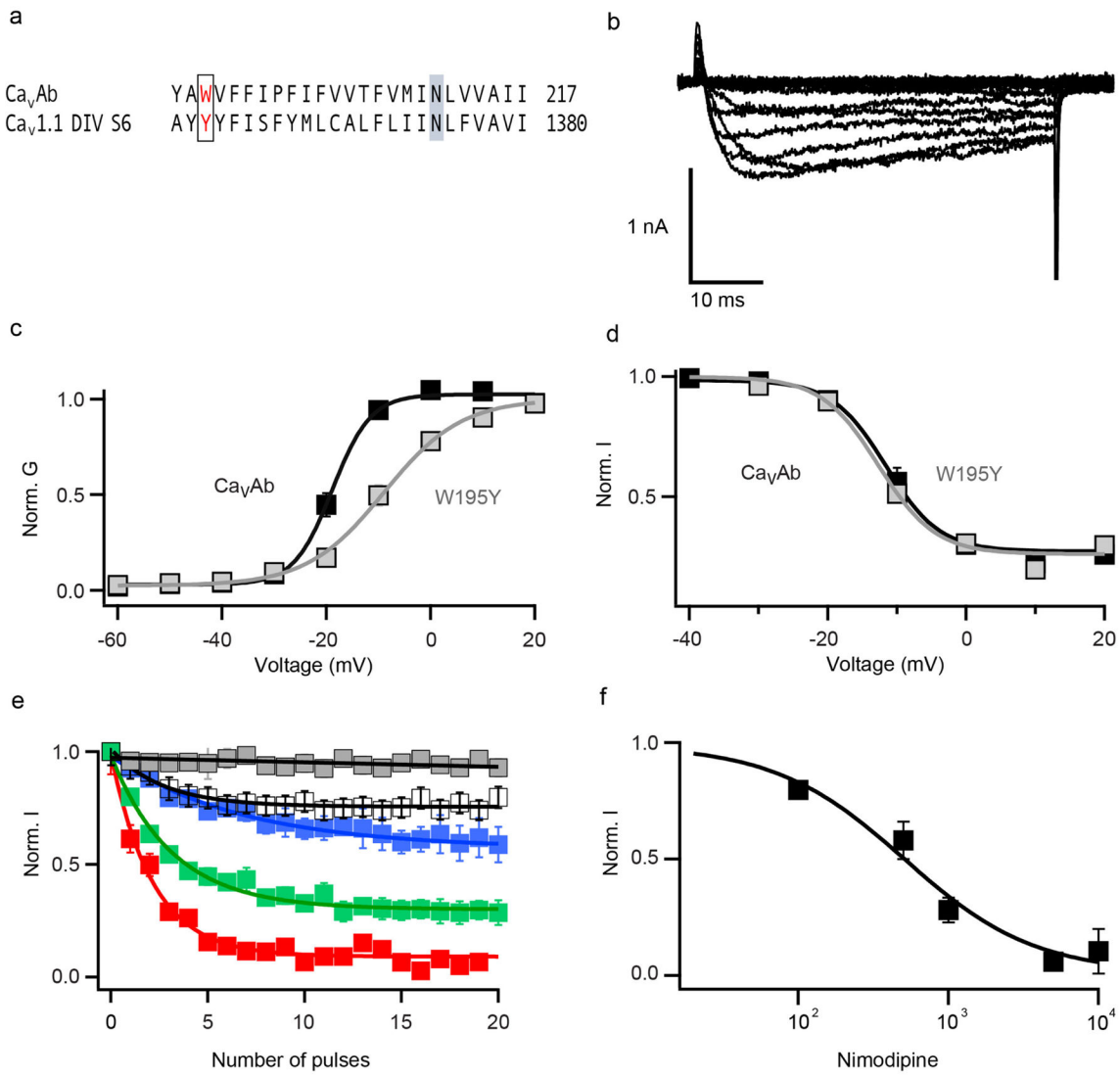

Extended Data Figure 3. Biophysical characterization and drug block of Ca_VAb W195 and Ca_VAb Y195

a, Sequence alignment of Ca_VAb S6 segment and Ca_V1.1 DIV S6. W195 in Ca_VAb is equivalent to Y1358 in Ca_V1.1. **b**, Ba2+ currents recorded from a holding potential of −120 mV to test potentials from 60 mV to 20 mV in 10 mV steps for Ca_VAb W195Y. **c**, *G–V* curves for Ca_VAb W195 and Ca_VAb Y195 derived from peak *I–V* relationships. The voltages for half-maximal activation and slopes are: Ca_VAb W195 $V_{1/2}$ = −18.8 ± 0.3, k = 3.7 ± 0.43, n = 7; Ca_VAb Y195, $V_{1/2}$ = −9 ± 0.3, k = 7.4 ± 0.1, n = 5. **d**, Steady-state inactivation of Ca_VAb W195 and Ca_VAb Y195 (n = 3). Two pulses were applied: a 300-ms conditioning pulse followed by 50-ms test pulse to 0 mV. **e**, State-dependent block of Ca_VAb W195Y by nimodipine at 100 nM (white), 500 nM (blue), 1 μM (green), 5 μM (red), and control (grey). **f**, Concentration-dependent block of Ca_VAb W195Y by nimodipine. IC_{50} = 508 ± 93 nM (n = 4–5 cells for each point).

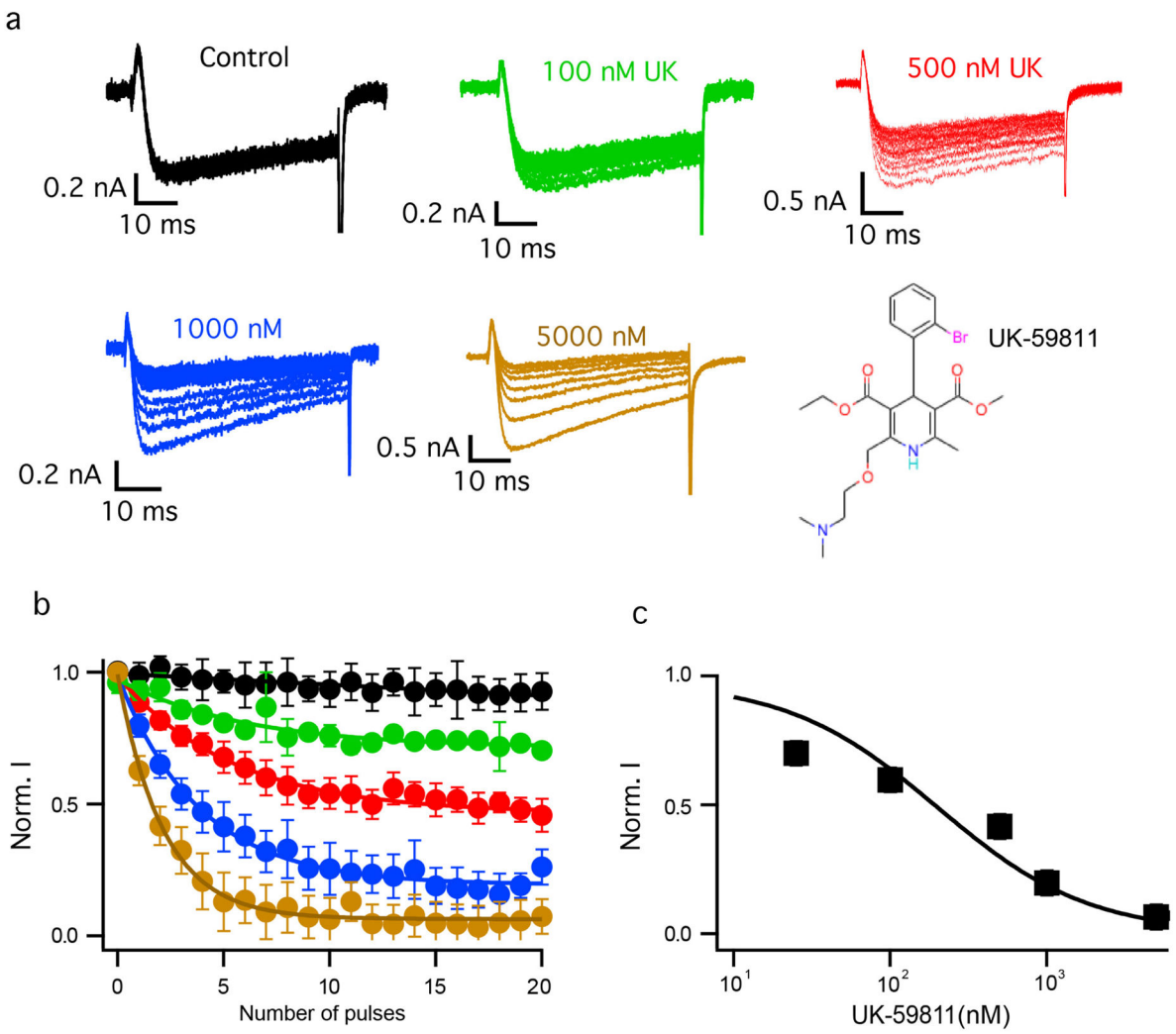

Extended Data Figure 4. Biophysical characterization of block by UK-59811

a, Ba^{2+} currents for state-dependent block by different concentrations of UK-59811. **b**, State-dependent block of Ca_VAb by UK-59811 at 0 nM (black), 100 nM (green), 500 nM (red), 1 μM (blue), and 5 μM (brown). For each curve, n = 4–5 cells. **c**, Concentration-response curve for UK-59811. Data were fit with a Hill equation assuming a 1:1 binding. IC_{50} = 194 ± 22 nM, n = 4–5.

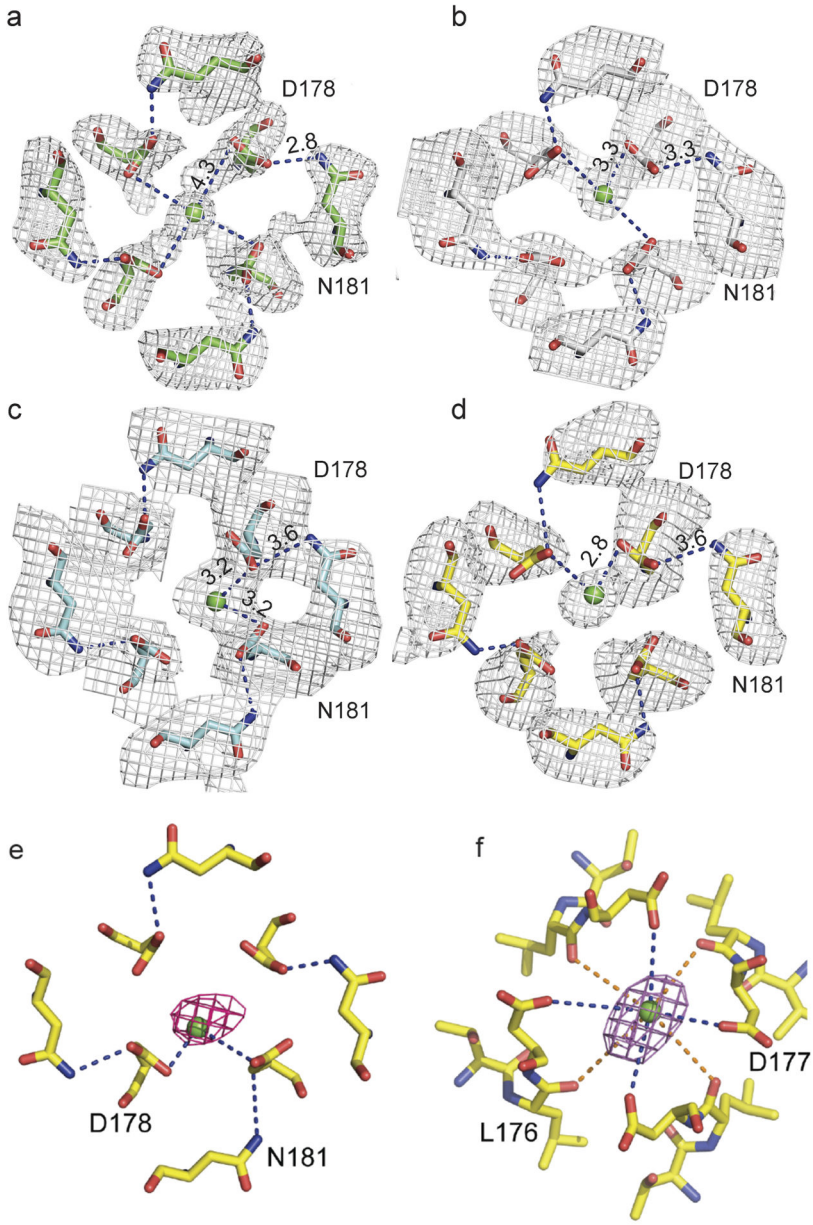

Extended Data Figure 5. Evidence for the partially dehydrated Ca^{2+} binding and carboxyl-carboxylate pairs at the selectivity filter entryway

a, Top view of an *F*o–*F*c simulated annealing omit map contoured at 3σ for residues 178 and 181 for the wild-type channel without drug. **b**, Top view of an *F*o–*F*c simulated annealing omit map contoured at 3σ for residues 178 and 181 for Ca_VAb–amlodipine. **c**, Top view of an *F*o–*F*c simulated annealing omit map contoured at 2.5σ for residues 178 and 181 for Ca_VAb–nimodipine. **d**, Top view of an *F*o–*F*c simulated annealing omit map contoured at 3σ for residues 178 and 181 for Ca_VAb– UK-59811. **e**, Top view of Site 1 with the anomalous difference Fourier map density (red mesh, contoured at 3σ) calculated with diffraction data of crystals collected at 1.75 Å wavelength. Ca^{2+} is shown as a green sphere. Site 1 residues are shown in sticks. Hydrogen bonds are indicated with dashed lines. **f**, Top

view of Site 2 with the anomalous difference Fourier map density (magenta mesh, contoured at 3σ).

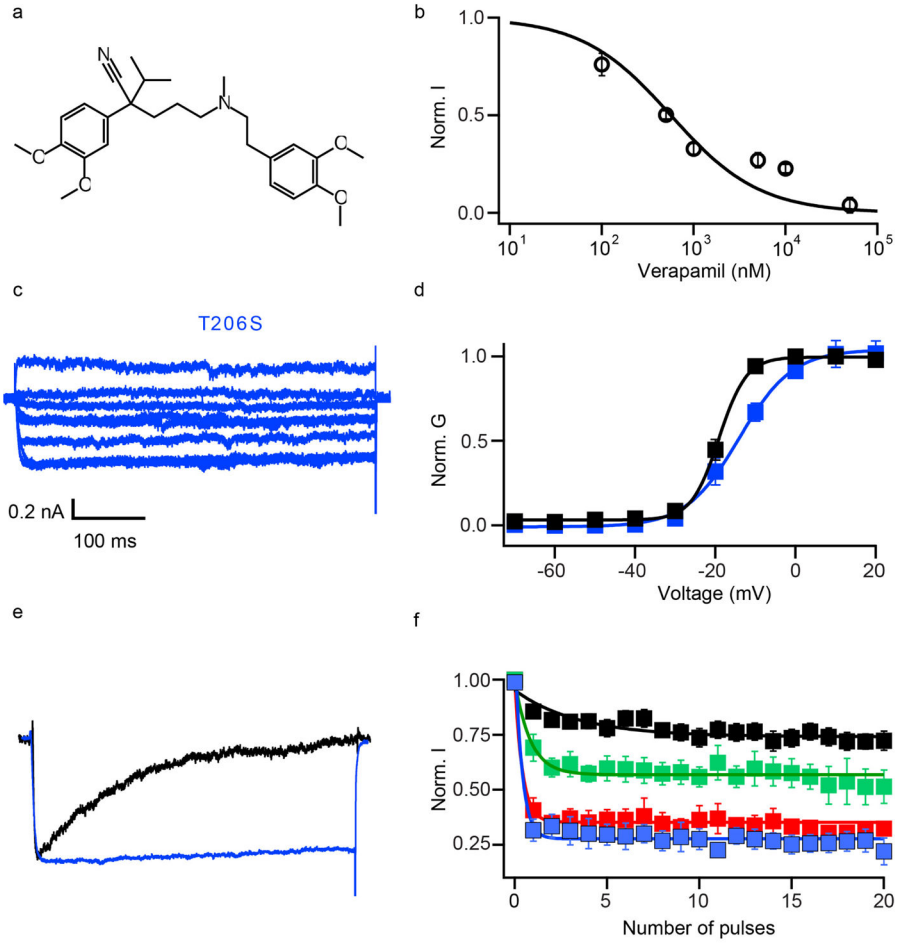

Extended Data Figure 6. Biophysical characterization of verapamil block of Ca_VAb and functional properties of Ca_VAb T206S

a, Chemical structure of verapamil. **b**, Concentration dependence of verapamil inhibition of Ca_VAb. The amplitude of the peak $Ba2^+$ current was recorded after applying 20 pulses at a frequency of 1 Hz, where the block reaches steady state. The data were fit by a Hill equation assuming a 1:1 binding ratio. n = 4–7 cells. IC_{50} = 475 ± 25 nM. **c**, Ba^{2+} currents of Ca_VAb T206S. **d**, G–V curves. Ca_VAb (black): $V_{1/2}$ = 18.8 ± 0.3 mV, k = 3.7 ± 0.43 (n = 5); Ca_VAb T206S (blue): $V_{1/2}$ = −15 ±1.8 mV, k = 6.6 ±0.4 (n =5). **e**, Current traces of Ca_VAb (black) and Ca_VAb T206S (blue) during a 1-s depolarizing pulse from a holding potential of –120 mV to −10 mV. **f**, State-dependent inhibition of Ca_VAb T206S by Br-verapamil at 10 μM (black), 25 μM (green), 50 μM (red), and 100 μM (blue). For each curve, n = 4–5 cells.

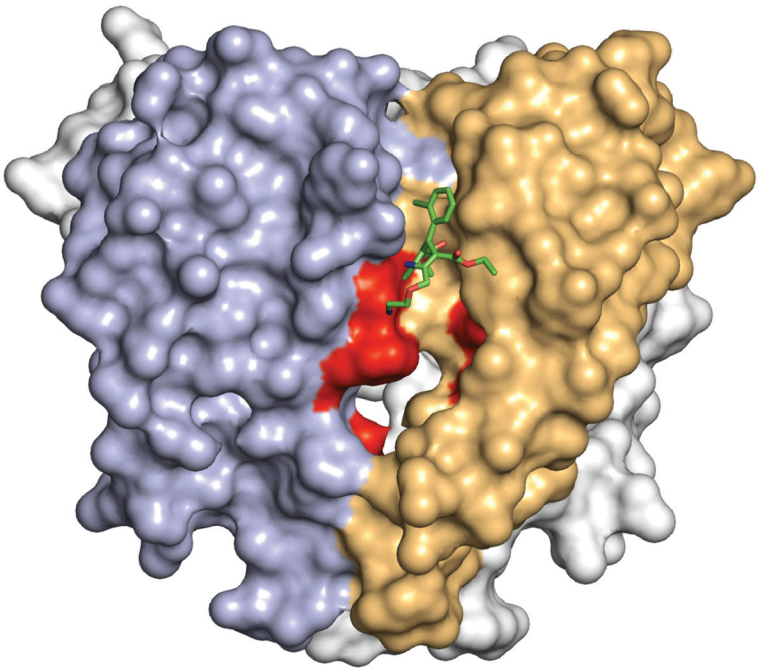

Extended Data Figure 7. Comparison of dihydropyridine binding site in Ca_VAb and $Ca_V1.2$

The pore domain of Ca_VAb is illustrated with two subunits in view, one in tan corresponding to domain III of $Ca_V1.2$ and one in blue corresponding to domain IV of $Ca_V1.2$. The amino acid residues in Ca_VAb corresponding to those that are important for dihydropyridine binding to $Ca_V1.2$ channels are highlighted in red. Bound amlodipine is illustrated with green sticks.

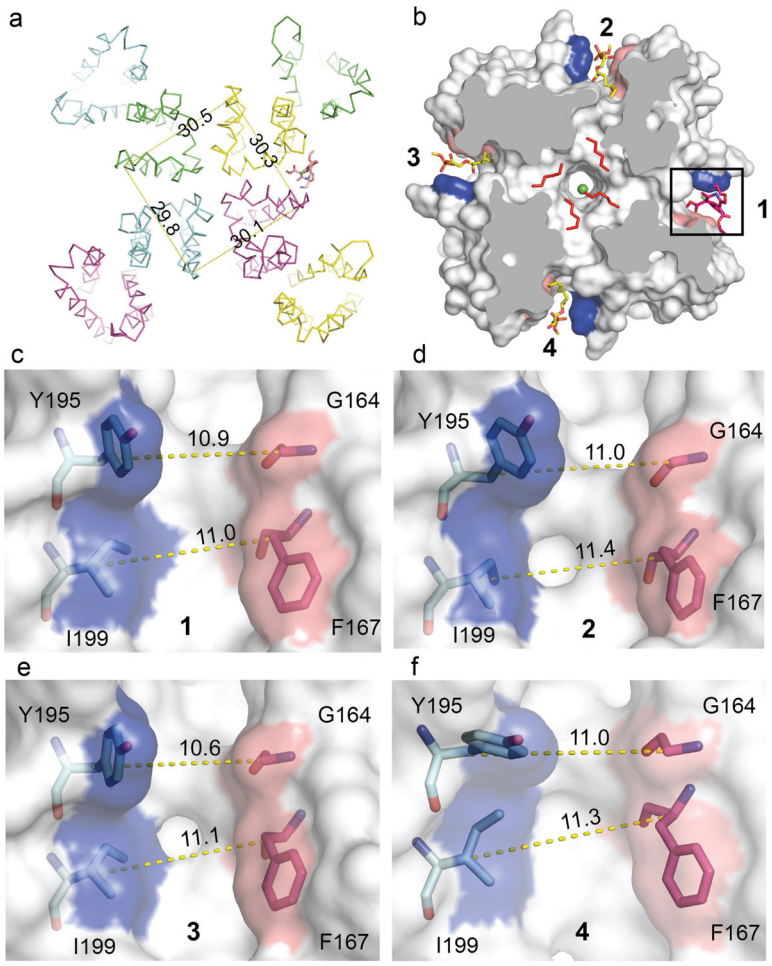

Extended Data Figure 8. Amlodipine binding breaks symmetry

a, The overall structure of Ca_VAb in complex with amlodipine (shown in ribbon representation). Measuring the C_α distances of V196 (nearing the amlodipine binding pocket) from the 4 subunits shows the channel is asymmetrical. **b**, Binding of amlodipine (sticks in red) induces asymmetry and causes rearrangement of the lipid in the central cavity. **c–f**, The amlodipine binding pocket showing the C_α–C_α distance at two layers (Y195–G164 and I199–F167) horizontally. At layer 1 (Y195–G164), the C_α–C_α distance of its neighbouring sites (11.0 Å in **d** and 11.0 Å in **f**) matches the drug binding site (10.9 Å in **c**), but the diagonal site (**e**) is too narrow (10.6 Å). At layer 2 (I199–F167), the pocket width of the diagonal site (11.1 Å in **e**) matches the drug-binding site (11.0 Å in **c**), but the two diagonal sites are too wide (11.4 Å in **d** and 11.3 Å in **f**).

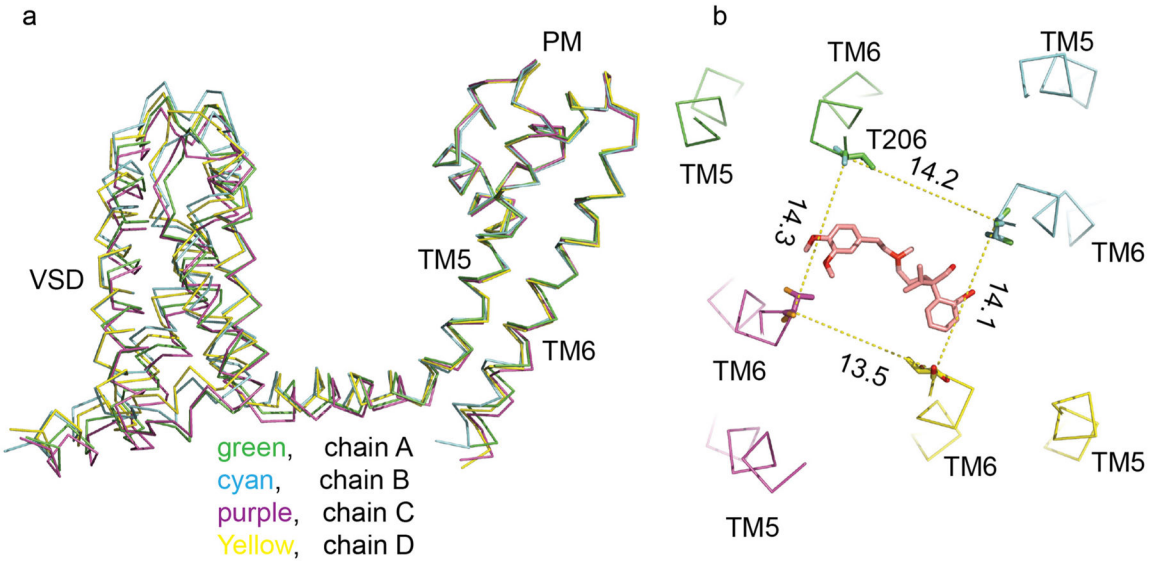

Extended Data Figure 9. Br-verapamil binding breaks symmetry

a, Alignment of the 4 subunits of Ca_VAb in complex with Br-verapamil showing the voltage sensor module (VSD) and the ends of S6 are different. **b**, Measuring the C_α distances between T206 residues in adjacent subunits shows that the channel is indeed asymmetrical with Br-verapamil in the pore.

Extended Data Table 1

Data collection, phasing and refinement statistics

	Ca_vAb 5mM Ca^{2+}	**Ca_vAb^1 (W195Y) UK-59811 5mM Ca^{2+}**	**Ca_vAb^2 UK-59811 5mM Ca^{2+}**	**Ca_vAb (W195Y) Amiodipine 5mM Ca^{2+}**	**Ca_vAb^1 (W195Y) Nimodipine 5mM Ca^{2+}**	**Ca_vAb^1 Br-verapamil 5mM Ca^{2+}**
Data collection						
Space group	P21221	P21221	P21221	P21221	P21221	P21221
Cell dimensions						
a, *b*, *c* (Å)	124.9 125.7 191.5	125.9 126.0 192.1	125.5 125.9 191.7	125.6 125.3 191.7	125.3 125.4 191.6	125.6 125.6 192
α,β,γ(°)	90 90 90	90 90 90	90 90 90	90 90 90	90 90 90	90 90 90
Resolution (Å)	2.7	3.3	3.3	3.2	3.2	3.3
R_{sym} or R_{merge}	11.4(98.4)	12.6(74.2)	11.7(60.1)	12.1(49.1)	11.2(68.6)	18.8(86.1)
$CC_{1/2}$(%)	99.8(87.7)	99.8(84.3)	99.7(87.4)	99.4(89.2)	99.7(86.7)	98.4(70.3)
//s/	13.4(2.4)	13.4(3.3)	13.1(3.1)	10.2(2.8)	15.2(3.5)	6.0(1.7)
Completeness (%)	92.5(97.8)	95.0(100.0)	92.1(82.0)	92.7(94.5)	99.8(99.8)	97.7(98.8)
Redundancy	10.1(9.8)	9.5(9.9)	9.4(9.2)	5.1(5.2)	9.3(9.0)	4.9(5.0)
Refinement						
Resolution (Å)	30-2.7	30-3.3	30-3.3	30-3.2	30-3.2	30-3.2

	Ca_vAb 5mM Ca^{2+}	Ca_vAb^1 (W195Y) UK-59811 5mM Ca^{2+}	Ca_vAb^2 UK-59811 5mM Ca^{2+}	Ca_vAb (W195Y) Amiodipine 5mM Ca^{2+}	Ca_vAb^1 (W195Y) Nimodipine 5mM Ca^{2+}	Ca_vAb^1 Br-verapamil 5mM Ca^{2+}
No. reflections	76513	46606	42515	46657	50390	49327
R_{work} / R_{free}	22.1/26.2	28.0/30.5	27.5/30.0	23.3/27.7	21.7/25.6	25.1/29.4
No. atoms	9684	7400	7403	7380	7393	7366
Protein	8780	7192	7200	7192	7192	7200
Ligand/ion	887	205	199	187	189	166
Water	17	3	2	1	28	
B-factors						
Protein	76.9	104.4	111.4	100.9	108.0	114.1
Ligand/ion	74.2	99.9	95.8	85.7	86.3	100.6
Water	46.6	57.9	63.2	48.8	52.8	
R.m.s deviations						
Bond lengths (Å)	0.009	0.013	0.013	0.013	0.013	0.013
Bond angles (°)	1.15	1.74	1.75	1.73	1.54	1.74
Ramachandran statistics						
Favored	96%	96%	96%	95.0%	96%	96.0%
Allowed	4.1%	3.6%	3.6%	4.6%	4.0%	4.1%
Outliers	0.28%	0.23%	0.23%	0.23%	0.12%	0.12%

[1]This data set is collected at 0.9198 Å.

[2]This data set is collected at 1.75 Å.

All other data sets are collected at 1.0 Å.

Acknowledgments

We are grateful to the beamline staff at the Advanced Light Source (BL8.2.1 and BL8.2.2) for their assistance during data collection. Research reported in this publication was supported by the National Heart, Lung, and Blood Institute (NHLBI) of the National Institutes of Health under award number R01 HL112808 (W.A.C. and N.Z.), and a National Research Service Award from training grant T32 GM008268 (T.M.S.). The content is solely the responsibility of the authors and does not necessarily represent the official views of the National Institutes of Health. This work was also supported by research grants from the Howard Hughes Medical Institute (N.Z.) and by the National Institute of Neurological Disorders and Stroke (NINDS) of the National Institutes of Health under award number R01 NS26254 (W.A.C.). D.C.P. acknowledges support from Neusentis, Pfizer Inc., Cambridge, UK during the course of this work.

References

1. Zamponi GW, Striessnig J, Koschak A, Dolphin AC. The physiology, pathology, and pharmacology of voltage-gated calcium channels and their future therapeutic potential. Pharmacol Rev. 2015; 67:821–870. [PubMed: 26362469]
2. Hondeghem LM, Katzung BG. Antiarrhythmic agents: the modulated receptor mechanism of action of sodium and calcium channel-blocking drugs. Annu Rev Pharmacol Toxicol. 1984; 24:387–423. [PubMed: 6203481]
3. Murphy KM, Gould RJ, Largent BL, Snyder SH. A unitary mechanism of calcium antagonist drug action. Proc Natl Acad Sci USA. 1983; 80:860–864. [PubMed: 6572372]
4. Catterall WA, Striessnig J. Receptor sites for Ca^{2+} channel antagonists. Trends Pharmacol Sci. 1992; 13:256–262. [PubMed: 1321525]

5. Hockerman GH, Peterson BZ, Johnson BD, Catterall WA. Molecular determinants of drug binding and action on L-type calcium channels. Annu Rev Pharmacol Toxicol. 1997; 37:361–396. [PubMed: 9131258]
6. Striessnig J. Pharmacology, structure and function of cardiac L-type Ca^{2+} channels. Cell Physiol Biochem. 1999; 9:242–269. [PubMed: 10575201]
7. Hofmann F, Lacinová L, Klugbauer N. Voltage-dependent calcium channels: from structure to function. Rev Physiol Biochem Pharmacol. 1999; 139:33–87. [PubMed: 10453692]
8. Cheng RC, Tikhonov DB, Zhorov BS. Structural model for phenylalkylamine binding to L-type calcium channels. J Biol Chem. 2009; 284:28332–28342. [PubMed: 19700404]
9. Tikhonov DB, Zhorov BS. Structural model for dihydropyridine binding to L-type calcium channels. J Biol Chem. 2009; 284:19006–19017. [PubMed: 19416978]
10. Takahashi M, Seagar MJ, Jones JF, Reber BF, Catterall WA. Subunit structure of dihydropyridine-sensitive calcium channels from skeletal muscle. Proc Natl Acad Sci USA. 1987; 84:5478–5482. [PubMed: 2440051]
11. Tanabe T, et al. Primary structure of the receptor for calcium channel blockers from skeletal muscle. Nature. 1987; 328:313–318. [PubMed: 3037387]
12. Mikami A, et al. Primary structure and functional expression of the cardiac dihydropyridine-sensitive calcium channel. Nature. 1989; 340:230–233. [PubMed: 2474130]
13. Wu J, et al. Structure of the voltage-gated calcium channel Cav1.1 complex. Science. 2015; 350:aad2395. [PubMed: 26680202]
14. Ren D, et al. A prokaryotic voltage-gated sodium channel. Science. 2001; 294:2372–2375. [PubMed: 11743207]
15. Catterall WA, Zheng N. Deciphering voltage-gated Na^{+} and Ca^{2+} channels by studying prokaryotic ancestors. Trends Biochem Sci. 2015; 40:526–534. [PubMed: 26254514]
16. Payandeh J, Scheuer T, Zheng N, Catterall WA. The crystal structure of a voltage-gated sodium channel. Nature. 2011; 475:353–358. [PubMed: 21743477]
17. Payandeh J, Gamal El-Din TM, Scheuer T, Zheng N, Catterall WA. Crystal structure of a voltage-gated sodium channel in two potentially inactivated states. Nature. 2012; 486:135–139. [PubMed: 22678296]
18. Zhang X, et al. Crystal structure of an orthologue of the NaChBac voltage-gated sodium channel. Nature. 2012; 486:130–134. [PubMed: 22678295]
19. Tang L, et al. Structural basis for Ca^{2+} selectivity of a voltage-gated calcium channel. Nature. 2014; 505:56–61. [PubMed: 24270805]
20. Catterall, WA.; Perez-Reyes, E.; Snutch, TP.; Striessnig, J. Voltage-gated calcium channels: introduction. IUPHAR/BPS Guide to Pharmacology. 2011. (http://guidetopharmacology.org/GRAC/FamilyIntroductionForward?familyId=80)
21. Striessnig J, Murphy BJ, Catterall WA. Dihydropyridine receptor of L-type Ca^{2+} channels: identification of binding domains for [^{3}H](+)-PN200-110 and [^{3}H]azidopine within the α1 subunit. Proc Natl Acad Sci USA. 1991; 88:10769–10773. [PubMed: 1660150]
22. Yamaguchi S, et al. Key roles of Phe1112 and Ser1115 in the pore-forming IIIS5-S6 linker of L-type Ca^{2+} channel α_{1C} subunit ($Ca_{V\,1.2}$) in binding of dihydropyridines and action of Ca^{2+} channel agonists. Mol Pharmacol. 2003; 64:235–248. [PubMed: 12869628]
23. Hescheler J, Pelzer D, Trube G, Trautwein W. Does the organic calcium channel blocker D600 act from inside or outside on the cardiac cell membrane? Pflügers Archiv. 1982; 393:287–291. [PubMed: 6289248]
24. Striessnig J, Glossmann H, Catterall WA. Identification of a phenylalkylamine binding region within the α1 subunit of skeletal muscle Ca^{2+} channels. Proc Natl Acad Sci USA. 1990; 87:9108–9112. [PubMed: 2174553]
25. Hockerman GH, Johnson BD, Scheuer T, Catterall WA. Molecular determinants of high affinity phenylalkylamine block of L-type calcium channels. J Biol Chem. 1995; 270:22119–22122. [PubMed: 7673189]
26. Yatani A, Brown AM. The calcium channel blocker nitrendipine blocks sodium channels in neonatal rat cardiac myocytes. Circ Res. 1985; 56:868–875. [PubMed: 2408778]

27. Kass RS, Arena JP, Chin S. Block of L-type calcium channels by charged dihydropyridines. Sensitivity to side of application and calcium. J Gen Physiol. 1991; 98:63–75. [PubMed: 1658191]
28. Bangalore R, Baindur N, Rutledge A, Triggle DJ, Kass RS. L-type calcium channels: asymmetrical intramembrane binding domain revealed by variable length, permanently charged 1,4-dihydropyridines. Mol Pharmacol. 1994; 46:660–666. [PubMed: 7969044]
29. Peterson BZ, Catterall WA. Calcium binding in the pore of L-type calcium channels modulates high affinity dihydropyridine binding. J Biol Chem. 1995; 270:18201–18204. [PubMed: 7629136]
30. Glossmann H, Ferry DR, Goll A, Striessnig J, Zernig G. Calcium channels and calcium channel drugs: recent biochemical and biophysical findings. Arzneimittelforschung. 1985; 35:1917–1935. [PubMed: 2420337]
31. Gamal El-Din TM, Martinez GQ, Payandeh J, Scheuer T, Catterall WA. A gating charge interaction required for late slow inactivation of the bacterial sodium channel NavAb. J Gen Physiol. 2013; 142:181–190. [PubMed: 23980192]
32. Faham S, Bowie JU. Bicelle crystallization: a new method for crystallizing membrane proteins yields a monomeric bacteriorhodopsin structure. J Mol Biol. 2002; 316:1–6. [PubMed: 11829498]
33. Faham S, et al. Crystallization of bacteriorhodopsin from bicelle formulations at room temperature. Protein Sci. 2005; 14:836–840. [PubMed: 15689517]
34. Otwinowski Z, Minor W. Processing of X-ray diffraction data collected in oscillation mode. Methods Enzymol. 1997; 276:307–326.
35. Collaborative Computational Project Number 4. The CCP4 suite: programs for protein crystallography. Acta Crystallogr D. 1994; 50:760–763. [PubMed: 15299374]
36. Brünger AT, et al. Crystallography & NMR system: a new software suite for macromolecular structure determination. Acta Crystallogr D. 1998; 54:905–921. [PubMed: 9757107]
37. Murshudov GN, Vagin AA, Dodson EJ. Refinement of macromolecular structures by the maximum-likelihood method. Acta Crystallogr D. 1997; 53:240–255. [PubMed: 15299926]
38. Adams PD, et al. PHENIX: a comprehensive Python-based system for macromolecular structure solution. Acta Crystallogr D. 2010; 66:213–221. [PubMed: 20124702]
39. Emsley P, Cowtan K. Coot: model-building tools for molecular graphics. Acta Crystallogr D. 2004; 60:2126–2132. [PubMed: 15572765]
40. Laskowski RA, Moss DS, Thornton JM. Main-chain bond lengths and bond angles in protein structures. J Mol Biol. 1993; 231:1049–1067. [PubMed: 8515464]
41. DeLano, WL. PyMol molecular viewer (V.1.2r3pre). 2002. (http://www.pymol.org)

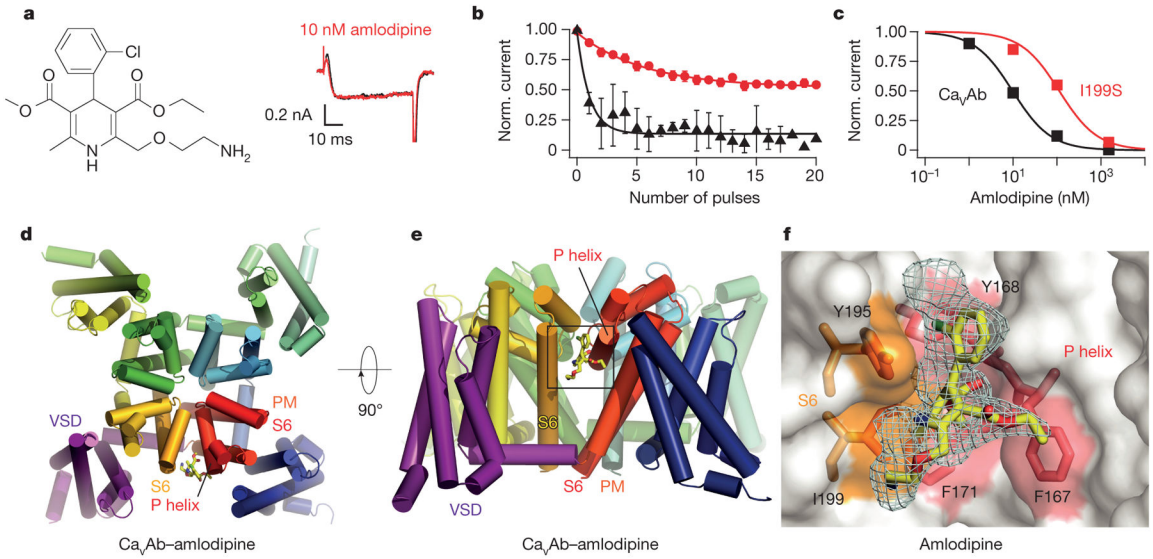

Figure 1. Structural basis for inhibition of Ca_VAb by amlodipine

a, Amlodipine structure. Ba^{2+} currents for 0 nM (black) and 10 nM (red) amlodipine during depolarization from −120 mV to 0 mV. **b**, State-dependent block by amlodipine after 50-ms pulses at 1 Hz from −120 mV to 0 mV (10 nM, circles; 100 nM, triangles; mean ± s.e.m.; n = 3–5. **c**, Inhibition by amlodipine. Data were fit by the Hill equation with n_H = 1. Ca_VAb: IC_{50} = 10 ± 0.4 nM; Ca_VAb I199S: IC_{50} = 112 ± 10 nM; n = 3–5; mean ± s.e.m. **d**, Structure of Ca_VAb (top view in cylinders) binding amlodipine (yellow sticks). PM, pore module; VSD, voltage-sensing domain. **e**, Ca_VAb with bound amlodipine in side view. **f**, Dihydropyridine-binding pocket of Ca_VAb with the F_o–F_c electron density map (2.5σ, cyan) and amlodipine (yellow sticks). Ca_VAb residues contacted by amlodipine are highlighted in colours and labelled.

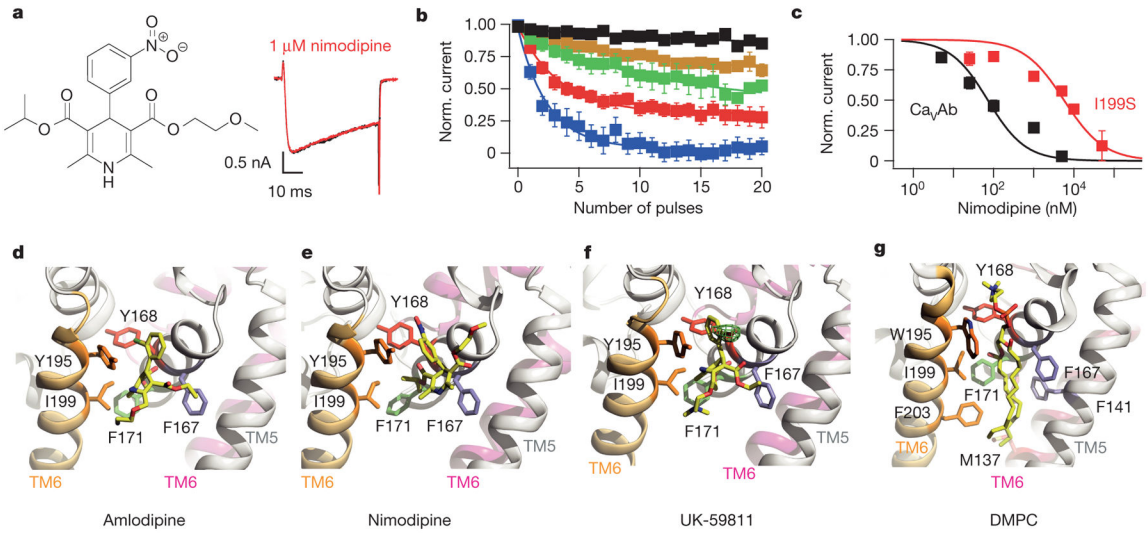

Figure 2. Inhibition of Ca_VAb by dihydropyridine binding at a lipid site

a, Nimodipine structure. Current records as in Fig. 1a. **b**, State-dependent block by nimodipine as in Fig. 1b: 5 nM (black), 25 nM (brown), 100 nM (green), 1 μM (red), and 5 μM (blue); mean ± s.e.m.; n = 3–14. **c**, Inhibition by nimodipine as in Fig. 1c. Ca_VAb: IC_{50} = 100±9 nM; Ca_VAb I199S, IC_{50} = 5.7±0.6μM; n = 3–14; means.e.m. **d**, Amlodipine (yellow sticks) bound to Ca_VAb. S5 and S6 helices in ribbons; residues surrounding amlodipine in sticks. **e**, Nimodipine bound to Ca_VAb. **f**, UK-59811 bound to Ca_VAb. Anomalous scattering density (3σ, green mesh) for Br in UK-59811. **g**, DMPC lipid in the drug-free dihydropyridine-binding site in yellow sticks.

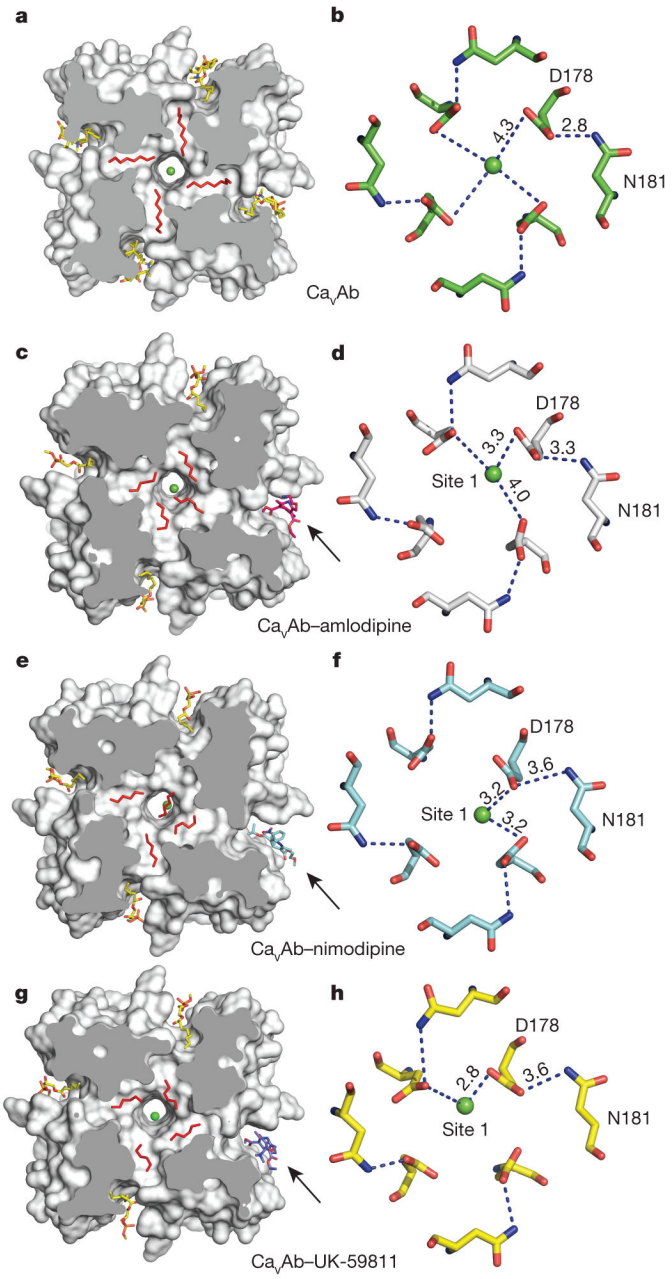

Figure 3. Dihydropyridine binding allosterically modifies Ca^{2+} binding in the selectivity filter

a, Outward view. Four symmetrical lipids (red sticks) occupy fenestrations in Ca_VAb without dihydropyridine. Four additional lipids bind to the side of the pore module (yellow sticks). **b**, Top view. Site 1 with hydrated Ca^{2+} (green) coordinated directly by D178 and indirectly by N181 on extracellular end of the selectivity filter. **c**, Amlodipine binding (magenta sticks) induces asymmetry and causes rearrangement of lipids (red sticks). **d**, Top view. Site 1 with partially dehydrated Ca^{2+} and direct interaction with D178 due to binding of amlodipine. **e**, Binding of nimodipine (cyan sticks) induces asymmetry and reorganizes bound lipid. **f**, Partially dehydrated Ca^{2+} binds at site 1 with coordination distance of 3.2 Å to carboxylate side chains of D178. **g**, Binding of UK-59811 (blue sticks) to the

dihydropyridine binding site induces asymmetry and reorganizes bound lipid. **h**, Ca^{2+} binds at Site 1 with coordination distance of 2.8 Å to a carboxylate side chain of D178.

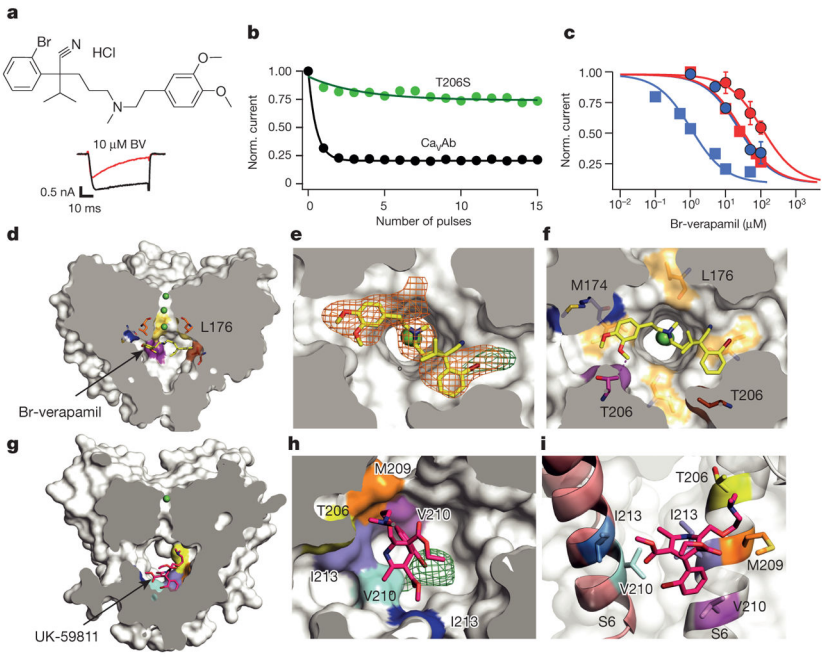

Figure 4. State-dependent inhibition by pore block with Br-verapamil and UK-59811

a, Br-verapamil. Ba^{2+} current records for Ca_VAb with 0 μM (black) and 10 μM (red) during the depolarizing pulse. **b**, State-dependent block of Ca_VAb (n = 7) and Ca_VAb T206S (n = 3) at 10 μM during trains of depolarizations at 1 Hz from −120 mV to 0 mV. The error bars for all the data points on this graph are too small to be visible. **c**, Inhibition by Br-verapamil for Ca_VAb and Ca_VAb T206S at V = −120 mV and following trains of depolarizations as in **b**. Ca_VAb: resting state block, blue circles, IC_{50} = 24 ±1.6 μM; state-dependent block, blue squares, IC_{50} =810 ±80 nM. Ca_VAb T206S: resting state block, red circles, IC_{50} = 115±3.2μM; state-dependent block, red squares, IC_{50} =24±0.8μM; n =3–11; mean ± s.e.m. **d**, Side view of the pore module sectioned through the selectivity filter with Br-verapamil bound (yellow sticks). Ca^{2+}, green spheres. **e**, F_o–F_c electron density (2.5σ, orange mesh) and anomalous scattering density (3σ, green mesh) for Br defines location of Br-verapamil. **f**, The two aromatic rings of verapamil are close to T206 of adjacent subunits. **g**, UK-59811 (red sticks) binds with its dihydropyridine ring deep in the central cavity. **h**, Anomalous scattering density (3.5σ, green mesh) of Br in UK-59811. **i**, S6 segments with residues surrounding UK-59811 in sticks.